

# Modification of alprazolam-induced liver injury by bone marrow-derived mesenchymal stem cells and the role of miRNA-192

Heba M. Ali Labib<sup>1,2</sup>

<sup>1</sup> Department of Anatomy and Embryology, Faculty of Medicine, Kasr Alainy, Cairo University, Egypt

<sup>2</sup> Department of Preclinical Science, College of Osteopathic Medicine, William Carey University, USA

## SUMMARY

The group of drugs known as Benzodiazepines (BDZs) are among the most widely prescribed CNS-depressant drugs. Alprazolam (Alp) is a member of the BDZs family, commonly prescribed as an antipsychotic and anxiolytic agent. Induction of oxidative stress, impairment of cognitive functions and psychomotor skills, conformational alterations in hemoglobin structure and elevation of liver enzymes are among the side effects reported on the use of alprazolam. Several studies have found that alprazolam could favor hepatotoxicity, whereas other studies contradicted those findings. Bone marrow-derived mesenchymal stem cells (BM-MSCs) have been studied as a novel approach for treatment of liver diseases. The current study was designed to assess the biochemical, histopathological and molecular liver alterations in response to oral administration of alprazolam at a dose of 0.3 mg/kg/day for 4 weeks in adult male albino rats and to evaluate the therapeutic effect of BM-MSCs on the alprazolam-induced alterations. Forty adult male albino rats (Sprague Dawley strain; 170-200 g mean body weight) were used. Liver enzymes were

measured, isolation and preparation of BM-MSCs were done, and immunohistochemical staining for alpha smooth muscle actin and FGF2 were assessed. Moreover, histological and ultrastructural liver tissue examination and PCR detection of SOD, TNF- $\alpha$  and mirNA-192 were investigated. Animals exposed to alprazolam developed liver injury characterized by significant increase in TNF- $\alpha$  and significant decrease in SOD and miRNA-192 expression. Histological findings provided supportive evidence for the biochemical and molecular analyses. Treatment with stem cells caused a significant alleviation of the alprazolam-induced findings. In conclusion, alprazolam was found to induce liver injury and oxidative stress, which were ameliorated by BM-MSCs administration.

**Key words:** Alprazolam – BMSCs – TNF- $\alpha$  – SOD – miRNA192

## INTRODUCTION

The prospects of morbidity and mortality escalate with drug abuse of prescription psychostimulants and depressants. Benzodiazepines (BZDs) are a group of psychoactive drugs that are recognized

### Corresponding author:

Heba Mohamed Ali Labib. Department of Anatomy and Embryology, Faculty of Medicine, Kasr Alainy, Cairo University, Egypt. Postal code, 11562. Province, Cairo. Address, 71 El Kasr Al Ainyy. Sector, Greater Cairo. Financial number, 1631. Phone: 02-2794782. E-mail: labib\_heba@yahoo.com

Submitted: May 7, 2022. Accepted: June 26, 2022

<https://doi.org/10.52083/IVLL6465>

for their anxiolytic, hypnotic and anticonvulsant properties and are extensively used in human pharmaco-therapy (Dinis-Oliveira, 2017).

Alprazolam is a benzodiazepine which is broadly used as an anxiolytic and an antipsychotic drug, as well as in the treatment of acute and sub-chronic insomnia and agitated psychosis (Zareifopoulo and Panayiotakopoulos, 2019). Alprazolam is metabolized in the liver, mainly by the enzyme cytochrome P450 3A4 (CYP3A4). Its maximum recommended daily dose is 10 mg per day (Uehara et al., 2017), whereas the median lethal dose (LD50) of alprazolam is 331-2171 mg/kg in rats (Golovenko et al., 2020).

Although once considered safe, several reports have emerged of alprazolam-induced multiple organ impairment. At a dose of 0.5 mg and higher, alprazolam caused alterations in brain oxidative metabolism and impairment of cognitive and psychomotor skills such as memory affection, with a substantial potential to prompt dependence and abuse. Alprazolam causes cytotoxicity in the vital organs of rats such as the liver and kidney (Chattopadhyay et al., 2019). Alprazolam is considered to be more toxic than other BZDPs. When co-administered with other depressant agents such as ethanol, alprazolam becomes particularly toxic, causing behavioral irritability and aggression (Huang et al., 2018). Chronic administration of alprazolam alone or with central nervous (CNS) stimulants increases oxidative stress and inflammation in the brain and induces neurobehavioral, histopathological and neurotransmitters levels' alterations (Dutt et al., 2020a). By means of spectrophotometry, alprazolam was shown to bind with hemoglobin (Hb), altering the  $\alpha$ -helical structure of Hb-subunits. Alprazolam-induced conformational changes in Hb result in changes of its function (Maitra et al., 2007).

Micro RNAs (miRNAs) are small non-coding RNAs which moderate gene expression by targeting 3' UTR of their related messenger RNA (mRNAs), playing a fundamental role in inflammation, carcinogenesis and cell death modulation. Whereas serum-based miRNAs are considered biomarkers in liver injury, several miRNAs expressed in liver tissue surpass the accuracy and sensitivity, as biomarkers, of serum aspartate

transaminase/alanine transaminase (AST/ALT) levels. miR-192 is proposed as a serum-based marker for acute liver injury. MicroRNA-192 (*miR-192-5p*) is expressed in the liver in a ubiquitous manner, and its expression has been examined in inflammation-related cancers. miR-192-5p is also considered to be a serum-based biomarker that is highly elevated in several liver diseases. In contrast, down-regulation of miR-192-5p in hepatocytes is seen upon liver damage, where its expression in hepatocytes is regulated by tumor necrosis factor  $\alpha$  (TNF- $\alpha$ ) (Roy et al., 2016).

In multicellular organisms, stem cells are undifferentiated or partially differentiated cells that have the ability to differentiate into various cell types and to proliferate indefinitely to produce more of the same stem cell. They are the initial type of cell in a cell lineage. They are found in both embryonic and adult organisms, with somewhat different properties in each. Stem cells are different from progenitor cells, which cannot divide indefinitely, and precursor or blast cells, which are usually committed to differentiating into one cell type (Müller et al., 2016).

Stem cells have the ability of long-term clonal self-renewal, by going through repetitive cycles of cell division while maintaining an undifferentiated state, and the ability of multipotency, with the capacity of differentiation into more than one specialized cell type (Kopp et al., 2016). Bone marrow-derived MSCs (BM-MSCs) are adult stem cells with multipotency and multilineage differentiation potential. BM-MSCs have the ability to differentiate into osteoblasts, chondrocytes, adipocytes, fibroblasts, endothelial cells, and smooth and cardiac muscle cells (Scuteri and Monfrini, 2018). In the adult liver, stem cells have been suggested to replace tissue cells, particularly following injury (Kopp et al., 2016).

The tumor necrosis factor (TNF) superfamily is a protein superfamily of type II transmembrane proteins containing TNF homology domain, which form trimers. Members of the TNF superfamily are freed from the cell membrane by extracellular proteolytic cleavage and function as cytokines. They are expressed by immune cells and they control various cell functions, such as immune response, inflammation, proliferation,

differentiation and apoptosis (Aggarwal et al., 2012). TNF- $\alpha$ -induced liver injury occurs via TNF-receptor-1 (TNFR1) signaling and TNFR1 inhibition markedly reduces liver steatosis and triglyceride content. Moreover, inhibition of TNFR1 reduces activation of the MAP kinase MKK7 and its downstream target JNK, leading ultimately to significant improvement in insulin resistance. Apoptotic liver injury, NAFLD activity and alanine aminotransferase (ALT) levels, as well as liver fibrosis are TNF- $\alpha$ -mediated and are decreased by anti-TNFR1 (Wandrer et al., 2020).

Superoxide dismutase (SOD) is an antioxidant enzyme that reduces superoxide radicals and protects against oxidative stress, through break down of H<sub>2</sub>O<sub>2</sub> into H<sub>2</sub>O and O<sub>2</sub>. In oxidative-stress-induced liver injury, SOD removes oxygen radical species and protects the integrity of the cells reducing production of reactive oxygen species (ROS) (Lim et al., 2021).

There are seven subfamilies of fibroblast growth factors (FGFs), FGF1 subfamily (FGF1, FGF2) being one of them. These subfamilies of FGFs are tissue specific and have different binding affinities with FGF receptors (FGFRs). Fibroblast growth factor 2 (FGF2) (also named basic FGF) possesses anti-fibrotic effects in liver fibrosis and enhance tissue regeneration. Activated hepatic stellate cells (HSCs) are the main cells responsible for extracellular matrix deposition; the distinctive feature of liver fibrosis. Among the fibroblast growth factor receptors (FGFRs), FGF2 chiefly interacts with FGFR1, highly overexpressed on activated HSCs, and inhibits HSCs' activation, migration and contraction and has thus been investigated in liver fibrosis. FGF2 also plays a critical role in numerous cellular processes including organ development, wound healing and tissue regeneration (Kurniawan et al., 2020).

Actins are a family of multi-functional proteins that form microfilaments. Alpha smooth muscle actin is one of six actin isoforms that are involved in the contractile apparatus of smooth muscles. Alpha-smooth muscle actin is related to hepatic dysfunction and the degree of liver fibrosis. As to its principal role in liver fibrogenesis,  $\alpha$ -SMA is one of the most useful immunohistochemical markers indicative of liver fibrosis, and is regarded as a

parameter of liver fibrogenesis. The expression of cytoplasmic  $\alpha$ -SMA is a histopathological marker for hepatic stellate cells (HSCs) activation responsible for liver fibrogenesis (Udomsinprasert et al., 2020).

It is probable that all psychopharmacological agents are accompanied with a risk of hepatotoxicity. However, the evidence is inadequate for certain conclusions to be drawn about the frequency and severity of psychiatric drug-induced liver injury. Prolonged use of BZDs is accountable for multiple side effects. The liver has a primary role in BZDs metabolism and is particularly prone to BZDs-related toxicity. Few data are available on the long-term impact of BZD administration on liver.

We herein investigate the potential toxic effects of alprazolam on enzymatic levels of Alanine aminotransferase (ALT) and Aspartate aminotransferase (AST) in rat serum. In addition, TNF- $\alpha$ , superoxide dismutase (SOD) and miRNA 192 in liver tissue homogenate are measured and correlated with liver injury with reference to molecular, histological and ultrastructural changes. Moreover, the protective role of mesenchymal bone marrow-derived stem cells against alprazolam-induced liver injury is examined.

## MATERIALS AND METHODS

### Animals

Forty adult male albino rats weighing (170-200 gm) were obtained from the Animal and Experimental House, Faculty of Medicine, Cairo University. Animals were housed in cages under standard hygienic conditions. All rats were acclimatized to the laboratory environment for two weeks prior to the experiment, where they were adapted to the controlled environmental conditions at a room temperature of 25 $\pm$ 2°C, relative humidity 60-70% under a 12h light: 12h dark cycle. All animals were subjected to a 1 hour fasting period prior to drug administration. Food and water were supplied ad libitum. All procedures were done in accordance with the principles of the Ethics Committee, Faculty of Medicine, Cairo University.

## Experimental design

The duration of the experiment was five weeks. Rats were equally and randomly divided into four groups (n=10 for each group); normal healthy group (group I), where the rats were housed separately in cages for five weeks without any manipulation; sham control group (group II), in which the rats were given a single intravenous (I.V.) injection ( $3 \times 10^6$  cell) of MSCs at the beginning of the fifth week; alprazolam group (group III), in which alprazolam was given daily as a single oral dose of 0.3 mg/kg/day for four weeks; and alprazolam+stem cells-treated group (group IV), in which alprazolam was given in a manner similar to that of group III, followed by a single I.V. injection ( $3 \times 10^6$  cell) of BM-MSCs at the beginning of the fifth week. All rats were sacrificed by the end of week five. All rats of the experiment were closely observed and carefully examined daily throughout the experimental period, in order to record any apparent behavioral changes and/or signs of toxicity. The dose for animal experimentation was calculated by extrapolating the human dose to animal dose based on the body surface area ratio following the table of Paget and Barnes (1964). The dose for alprazolam was recommended by Elmesallamy et al. (2011) and was assessed in its maximum therapeutic dose used for treatment of generalized anxiety disorders.

## Chemicals

Alprazolam in the form of white crystalline powder was obtained from Amoun Pharmaceutical Industries Co., Egypt, freshly prepared for oral gavage administration by dissolving it in distilled water (each 0.5 mg dissolved in 5 ml of distilled water).

## Preparation of BM-derived MSCs (BMSCs)

Bone marrow was harvested from 6-week-old male white albino rats by flushing the tibiae and femurs with Dulbecco's modified Eagle's medium (DMEM, GIBCO/BRL), supplemented with 10% of fetal bovine serum (GIBCO/BRL). Nucleated cells were isolated with a density gradient [Ficoll/Paque (Pharmacia)] and suspended in complete culture medium supplemented with 1% of penicillin-streptomycin (GIBCO/BRL). Cells were incubated

at 37°C in 5% of humidified CO<sub>2</sub>. When large colonies developed (80–90% confluence), cultures were washed twice with phosphate-buffered saline (PBS, Lonza Company, Switzerland) and the cells were trypsinized with 0.25% of trypsin in 1mM EDTA (GIBCO/BRL) for 5 min at 37°C. Cells were centrifuged and suspended in serum supplemented medium and incubated in 50 cm<sup>2</sup> culture flask (Falcon, Nunc, Roskilde, Denmark). MSCs were identified by their adherence to the plastic surface.

## Labeling of MSCs with PKH26

PKH26 fluorescent linker dye was used for MSCs labeling according to Sigma Protocol (St. Louis, MO). Briefly, cells were centrifuged and washed twice in serum free medium. Cells were pelleted and suspended in dye solution and then were injected intravenously into the tail vein.

## Biochemical analysis

The blood samples were collected from the tail vein for biochemical testing of serum alanine aminotransferase (ALT) and aspartate aminotransferase (AST) at 8:00 a.m. at the end of the 5<sup>th</sup> week. The blood samples were then centrifuged at 3000g for 10 min using a bench top centrifuge (KH20R, Kaidalab, China). The sera acquired from the sample tubes were stored frozen at -80°C to be used for analysis at a later time. Afterwards, all animals were anesthetized by use of sodium pentobarbital (40 mg/kg, i.p.) and decapitated after reaching full anesthesia according to the guidelines of the Institutional Animal Care and Use Committee (IACUC). Serum activities of ALT and AST were used to evaluate the liver function.

## Histopathological analysis

The liver was rapidly isolated and immersed in freshly prepared 4% w/v formaldehyde (0.1 M phosphate buffers, pH7.2) for 48h and then embedded in paraffin with melting point 55–57°C. 4µm-thick histological sections were prepared and stained with hematoxylin and eosin for routine histological study and with Masson's trichrome for detection of collagen fiber deposition. Capturing images for microscopic

analysis was performed using light microscope model DM LB2 (Switzerland).

Sections for immunohistochemical study were mounted on charged slides to help adherence of sections to the slides during immunostaining. Immunostaining was done for fibroblast growth factor 2 (FGF2) and alpha smooth muscle actin ( $\alpha$ -SMA).

### **Processing of specimens and stains for light microscopy**

Hematoxylin and eosin staining entailed deparaffinization of sections in xylene followed by rehydration in descending grades of ethanol. The sections were stained with hematoxylin for 10 minutes, bluing in tap water was then done, followed by staining with eosin for 1 minute. Sections were cleared in xylene then mounted on slides and covered.

For Masson's trichrome staining, the fixed paraffin sections were stained with Trichrome Stain Kit (Connective Tissue Stain) (ab150686). Sections were deparaffinized and the slides were incubated in preheated Bouin's Fluid then in Weigert's Iron Hematoxylin and rinsed in water. Afterwards, incubation in Biebrich Scarlet/Acid Fuchsin solution was done and the slides were differentiated in phosphomolybdic / phosphotungstic acid solution. Further incubation in Aniline Blue solution for 5-10 minutes and in acetic acid solution followed. Sections were cleared in xylene and mounted in permanent mounting medium.

### **Fibroblast Growth Factor 2 (FGF2) immunohistochemical analysis**

To perform antibody staining, deparaffinization and rehydration were initially done, followed by antigen unmasking. Afterwards, staining was performed using the chromogenic staining protocol. To prevent non-specific binding of the antibody to the tissues, each section was blocked with 100-400  $\mu$ l blocking solution for 1 hour at room temperature in a humidified chamber. The blocking solution was removed and 100-400  $\mu$ l of primary antibody *FGF2 Mouse Polyclonal Antibody* (Cat #: [PMA5-15276](#)), *ThermoFisher Scientific*,

*USA*, was added. Equilibration with Signal Stain Boost Detection Reagent and addition of Signal Stain DAB Chromogen Concentrate and Signal Stain DAB Diluent were done. The final step was counterstaining with hematoxylin, which stains the cell nuclei blue, providing a contrast to the brown color of the DAB chromogen for better visualization of tissue morphology.

### **Alpha smooth muscle Actin ( $\alpha$ -SMA) immunohistochemical analysis**

To perform antibody staining, deparaffinization and rehydration were initially done. The sections were mounted on glass slides coated with 0.1% poly-1-lysine. Subsequent blockage of the endogenous peroxidase activity, by incubation in 2.5% methanolic hydrogen peroxide for 30 minutes, was performed. The endogenous biotin was blocked by Biotin Blocking System (Agilent, CA, USA), according to the manufacturer's instructions. Subsequently, the sections were washed three times in phosphate-buffered saline (PBS). The blocking solution was removed and 100-400  $\mu$ l of primary antibody *Mouse Anti-Alpha Smooth Muscle Actin Monoclonal Antibody (Clone 1A4)* (CAT#: [NAB201062LS](#)), *Creative Biolabs, NY, USA*, was added. After three washings in PBS, the sections were incubated for 30 minutes with the appropriate secondary biotinylated antibody labelled with Avidin-Biotin complex (*ThermoFisher Scientific, USA, code 29339*). The sections were developed with 3-3 diaminobenzidine and finally counterstained with hematoxylin. Negative controls were performed using normal house antiserum instead of the primary antibody, which uniformly demonstrated no reaction.

### **Immunohistochemistry data interpretation**

The evaluation of immunostaining was performed using *OptikalSView camera software, Optika, Italy*. The immune-positive cells were counted in each region of interest (ROI) using a counting grid in relation to their proportion among the total counterstained cell population. The stained areas of the ROI were digitally marked, and the percentage of stained areas was determined and the staining intensity scored according to a four-tier system: 0, no staining;

1+, weak; 2+, moderate; and 3+, strong. In brief, the score of each sample was calculated as the sum of each intensity (0–3) multiplied by the percentage of positive cells (0–100%) determined by immunohistochemistry (IHC). The specimens were immediately examined then stored at 4°C protected from light for long term storage. The microscopic examination was performed by *LABOMED Fluorescence microscope LX400, cat no: 9126000; US*. Using the aforementioned staining scores, the positive areas of positive cells of FGF2 and  $\alpha$ -SMA were determined by measuring at least 7–10 randomly selected microscopic fields on each slide. The number of FGF2 and alpha-SMA-positive cells was counted under light microscope at 400 magnifications: only the cells which displayed nuclei on the section were considered.

### Processing of specimens for electron microscopy

Transmission electron microscopy (TEM) lab was performed at Cairo University Research Park – Faculty of Agriculture (CURP). Ultra-thin tissue sections were examined by transmission electron microscope JEOL (JEM-1400 TEM) at the candidate's magnification. Images were taken by CCD camera model AMT, optronics camera with 1632 x 1632 pixel format as side mount configuration which uses 1394 fire wire board for acquisition. Microtome sections were prepared at approximately 500–1000 nm thickness with a Leica Ultracut UCT ultramicrotome. The sections were stained with toluidine blue (1X), then sections were examined by Leica ICC50 HD camera. For tissue processing, specimens were cut into 1–2 mm<sup>3</sup> thick pieces, then instantly fixed in 3% glutaraldehyde formol (v/v) in 0.1 M sodium phosphate buffer (pH 7.2–7.4) over night at 4°C. Specimens were additionally processed by washing in buffer, post fixed in 1% osmium tetroxide, washed in 4 changes of distilled water and dehydrated in ascending grades of ethanol. Next, embedding in Epoxy resin and embedding of the specimens in beam capsules followed. The specimens were sectioned on LKB ultramicrotome utilizing glass knives for ultrathin sections. Ultrathin sections of 0.6–0.8  $\mu$ m in thickness were acquired from selected blocks, then mounted on copper grids and doubly stained with uranyl

acetate and lead citrate. Electron micrographs were taken with clear linear images and without angles or artifacts.

### Reverse transcription-real time quantitative PCR for TNF- $\alpha$ , SOD and miRNA 192

Total RNA and miRNA extraction and purification were done from paraffin-embedded tissue using the RNeasy FFEP Kit; cat no: 73504 (Qiagen, Hilden, Germany) according to the manufacturer's protocol. Reverse transcription, in which cDNA was synthesised by reverse transcription reaction using miScript RT-II Transcription Kit; cat no: 218160; (Qiagen, Hilden, Germany) was done. Gene expression analysis was performed by the quantification of TNF- $\alpha$  and SOD genes levels, which were amplified from mRNA using a QuantiTect primer assay primer assays; [Rn\_TNF- $\alpha$ \_1\_SG QuantiTect Primer Assay; cat no: 249900, and Rn\_SOD\_1\_SG QuantiTect Primer Assay, cat no: 249900] respectively and the QuantiTect SYBR Green PCR Kit cat no: 204141 (Qiagen, Germany). The ACTB Primer sequence was used as housekeeper gene. All samples were analyzed using the 5 plex Rotor-Gene PCR Analyzer (Qiagen, Germany). The 2<sup>ΔΔCt</sup> method was conducted for the analysis of gene expression levels, using ACTB as an endogenous reference control for normalization purposes. miRNA 192 expression analysis was performed by the quantification of miR-192 expression level using the SYBR-Green fluorescent-based primer assay (Rn\_miR-192\*\_1 miScript primer assays, assay ID: MIMAT0017147, Qiagen, Germany). The used miRNA sequence was: 5'CUGCCAGUCCAUAGGUCACAG-3'. The RUN6 primer assay was used as housekeeper gene for normalization. The qPCR was performed in the 5-plex Rotor Gene PCR System (Qiagen, Hilden, Germany). The 20  $\mu$ l reaction mixture / reaction consist of 2x QuantiTect syber green PCR mastermix, 10x miscript universal primer, 2  $\mu$ l primer assay and 50pg–3ng cDNA. The thermal protocol for the target gene consisted of 15 min for HotStarTaq DNA Polymerase activation at 95°C followed by 40 cycles of denaturation at 94°C for 15 minutes, primer annealing for 30 seconds at 55°C and extension at 70°C for 30 sec). The

2<sup>ΔΔ</sup>Ct method was conducted for the analysis of miR-192 expression levels, using RUN6 as an endogenous reference control for normalization purposes.

### Data Analysis

Data were statistically described in terms of mean ± standard deviation (±SD). Data were tested for the normal assumption using the Shapiro-Wilk test. Comparison of the study groups was done using one way analysis of variance (ANOVA) test with posthoc multiple 2-group comparisons. Two-sided *p* values < 0.05 were considered statistically significant. All statistical calculations were done using computer program IBM SPSS (Statistical Package for the Social Science; IBM Corp, Armonk, NY, USA) release 22 for Microsoft Windows.

## RESULTS

### Biochemical Results

There was no statistically significant difference in ALT and AST mean serum levels between the control groups I and II. Also, a non-significant difference was seen between the controls and the alprazolam-treated group III. In addition, there was not sufficient statistical evidence to suggest a significant difference between the alprazolam+stem cells-treated group IV and neither the controls nor the alprazolam-treated group III (Table 1).

**Table 1.** Effect of alprazolam and alprazolam+stem cells on ALT (U/L) and AST (U/L) serum levels as compared to the controls, represented as mean ± SD.

	Group	Mean ± SD	Versus	p-value
	ALT	I	33.92±3.7	Group II Group III Group IV
II		34.10±2.4	Group I Group III Group IV	1.000 0.084 0.092
III		35.31±6.9	Group I Group II Group IV	0.080 0.084 0.079
IV		34.63±8.1	Group I Group II Group III	0.087 0.092 0.079
	Group	Mean ± SD	Versus	p-value
	AST	I	108.13±11.4	Group II Group III Group IV
II		108.81±9.3	Group I Group III Group IV	1.000 0.089 0.094
III		109.43±7.5	Group I Group II Group IV	0.083 0.089 1.000
IV		109.17±3.7	Group I Group II Group III	0.090 0.094 1.000

\**p* value ≤ 0.05 was deemed statistically significant; SD=standard deviation.

### Fluorescence results

Florescent microscopic examination of the unstained sections of liver in the sham control group (II) and in the alprazolam +stem cells treated-group (IV) displayed homing of PKH26 labeled MSCs in the liver tissue (Fig. 1).

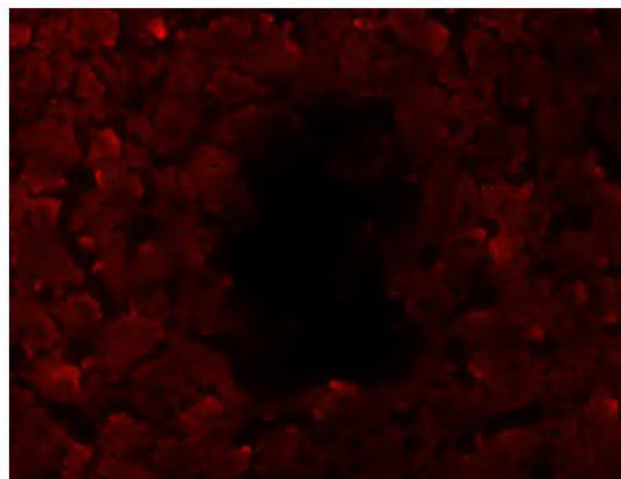
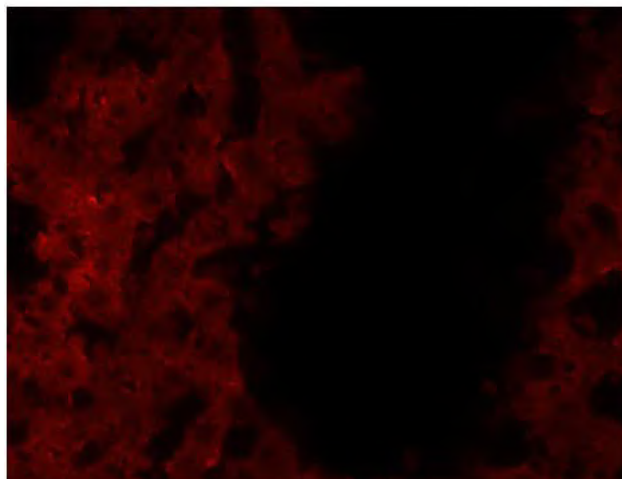


**Fig. 1.-** PKH26-labeled injected stem cells of the unstained sections of the rat liver in a. sham control group II and b. alprazolam + stem cells-treated group IV showing engraftment of MSCs and their homing in the hepatocytes.

## Histopathological Results

### *Hematoxylin and eosin staining*

The hepatic parenchyma of the controls' rats depicted hepatic lobules separated from one another by connective tissue septa where portal areas accommodated the portal triad. Each hepatic lobule featured a central vein from which hepatic plates radiated. The portal areas included a hepatic portal vein, a branch of the hepatic artery and a bile ductile (Figs. 2a and b, 3a and b and 4). Treatment with alprazolam caused focal necrosis, inflammatory cellular infiltration, hepatocyte vacuolization and nuclear pyknosis with sinusoidal dilatation (Figs. 1c, 2c and d and 5a, b). An apparent restoration of hepatic architecture was noticed in the liver of alprazolam+stem cells-treated rats (Figs. 2d, 3e and 5c).

### *Masson's trichrome staining*

Normal liver staining was seen in control and sham control groups I and II (Fig. 6a, b). Pericentral and periportal collagen fibers deposition were seen in alprazolam-treated liver sections (Fig. 6c, d) as indicated by strong blue staining which was apparently reduced in the alprazolam+stem cells-treated stained section (Fig. 6e).

### *Immunohistochemical Staining*

Very faint FGF-2 immune-expression was present in control groups I and II (Fig. 7a, b). Strong FGF-2 immune-expression was seen in alprazolam-treated sections (Fig. 7c), as indicated by strong and diffuse brown staining of hepatic parenchyma especially noticed pericentrally. A faint expression was seen in alprazolam+stem cells-treated liver sections (Fig. 7d).

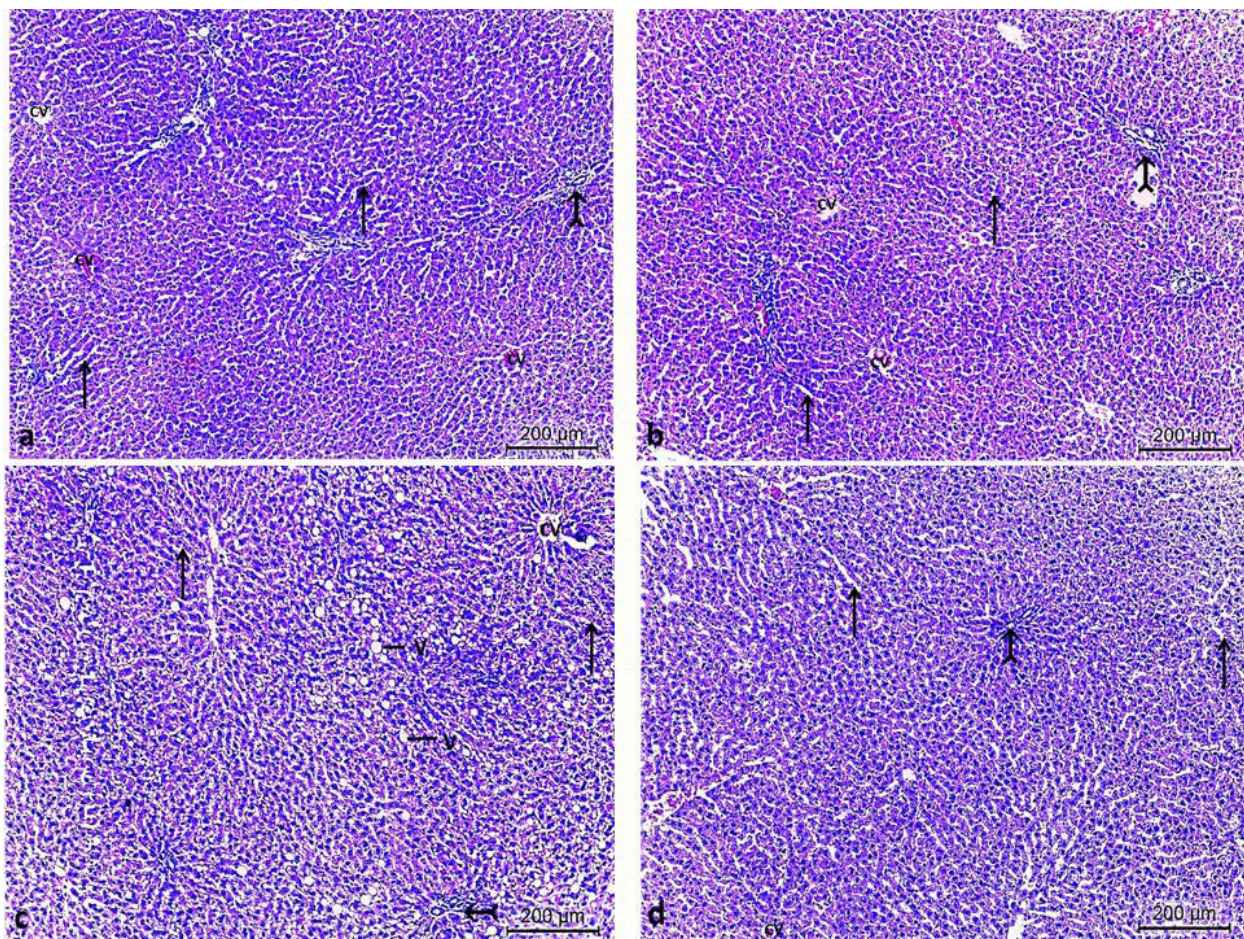


**Fig. 2.-** Hematoxylin and eosin-stained sections of rat liver in **a.** control and **b.** sham control groups I and II illustrating numerous hepatic lobules, in the center of each is the central vein (CV). The hepatic sinusoids (arrow) appear between the plates of hepatic cells that radiate from the central veins toward the periphery of the hepatic lobule. Branches of the interlobular vessels and bile ducts are seen within the portal areas (tailed arrow) of a hepatic lobule. **c.** Hematoxylin & Eosin-stained sections in alprazolam-treated rat liver showing ballooning and vacuolization (V) of hepatocytes. **d.** Alprazolam+Stem Cells-treated rat liver featuring central vein (CV), hepatic sinusoids (arrow) and branches of the interlobular vessels and bile ducts within the portal areas (tailed arrow) of a hepatic lobule. H&E staining, x100. Scale bars = 200 μm.

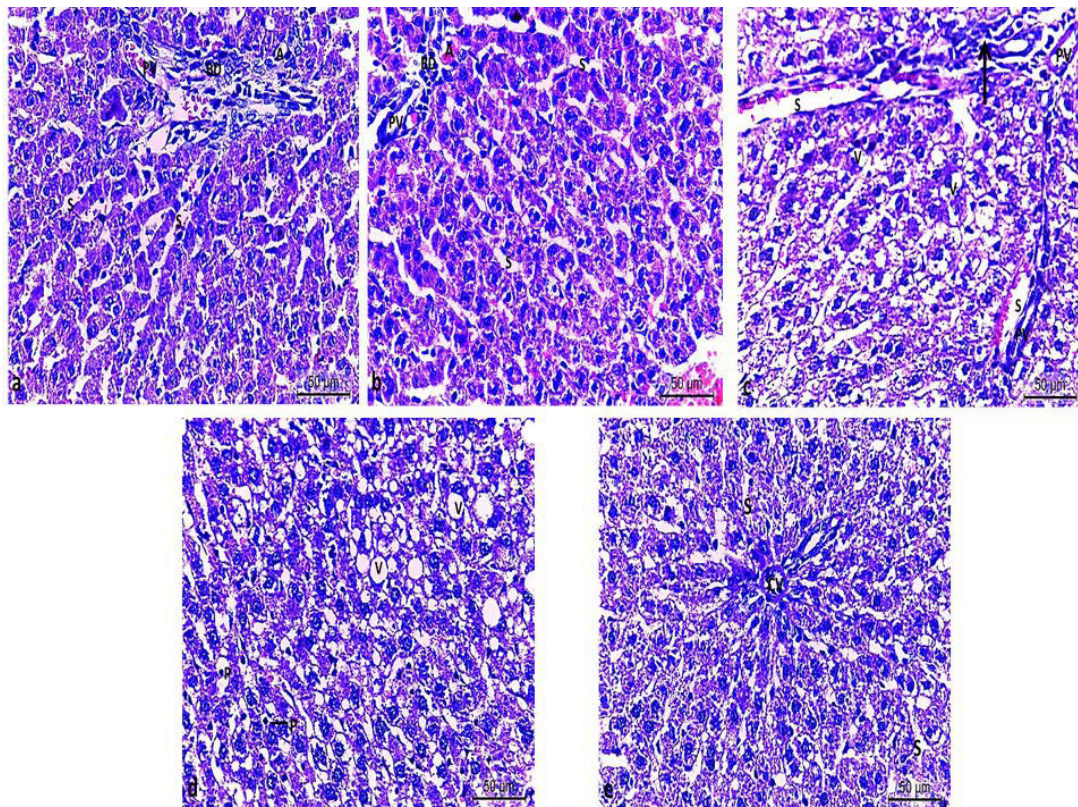


**Fig. 3.-** Hematoxylin and eosin-stained sections of rat liver. **a.** Liver of control group I and **b.** of sham control group II exhibiting normal architecture. Blood sinusoids (S) intervening between regularly arranged plates of hepatic cells radiate from central veins (CV). Branches of the interlobular vessels; portal vein (PV) and hepatic artery (A), in addition to bile ducts (BD) are seen within the portal areas. **c** and **d.** Liver of alprazolam-treated group III exhibit areas of focal necrosis and intra-lobular mononuclear inflammatory infiltration (arrow), identified around portal veins (PV), dilatation of sinusoids (S), hepatocyte nuclear pyknosis (P) vacuolar degeneration and atrophy of hepatocytes (V) with loss of hepatic architecture. **e.** Liver of alprazolam+stem cells-treated group IV featuring restoration of normal architecture. Blood sinusoids (S) intervene between plates of hepatic cells which radiate from a central vein (CV). H&E, x400. Scale bars = 50 µm.

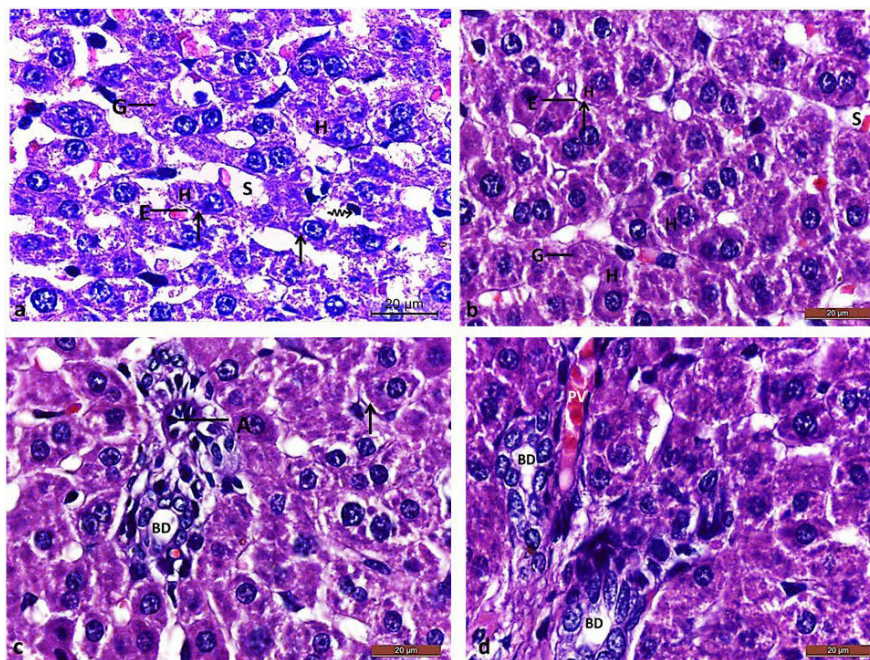


**Fig. 4.-** Hematoxylin and eosin-stained sections of rat liver in **a.** control group I and **b.** sham control group II showing normal hepatic architecture. Hepatocytes (H) are arranged in plates, between which the sinusoids (S) are situated. The space of Disse (arrow) is visible and appears as a thin bright band between hepatocyte cytoplasm (H) and the thinner, darker band which represents the endothelium (E) where the endothelial cells have flattened nuclei. Glycogen granules are also seen within the hepatocyte cytoplasm (G). Kupffer cells can be recognized by their several processes and an irregular or stellate outline that protrudes into the sinusoids closely associated with sinusoidal spaces (zigzag arrow). Cross section in rat liver stained with H&E in **c.** control and **d.** sham control groups I and II showing the portal area of the hepatic lobule. Branches of the portal vein (PV), bile duct (BD) and hepatic artery (A) are seen as well as space of Disse (arrow). H&E, x1000. Scale bars = 20 µm.

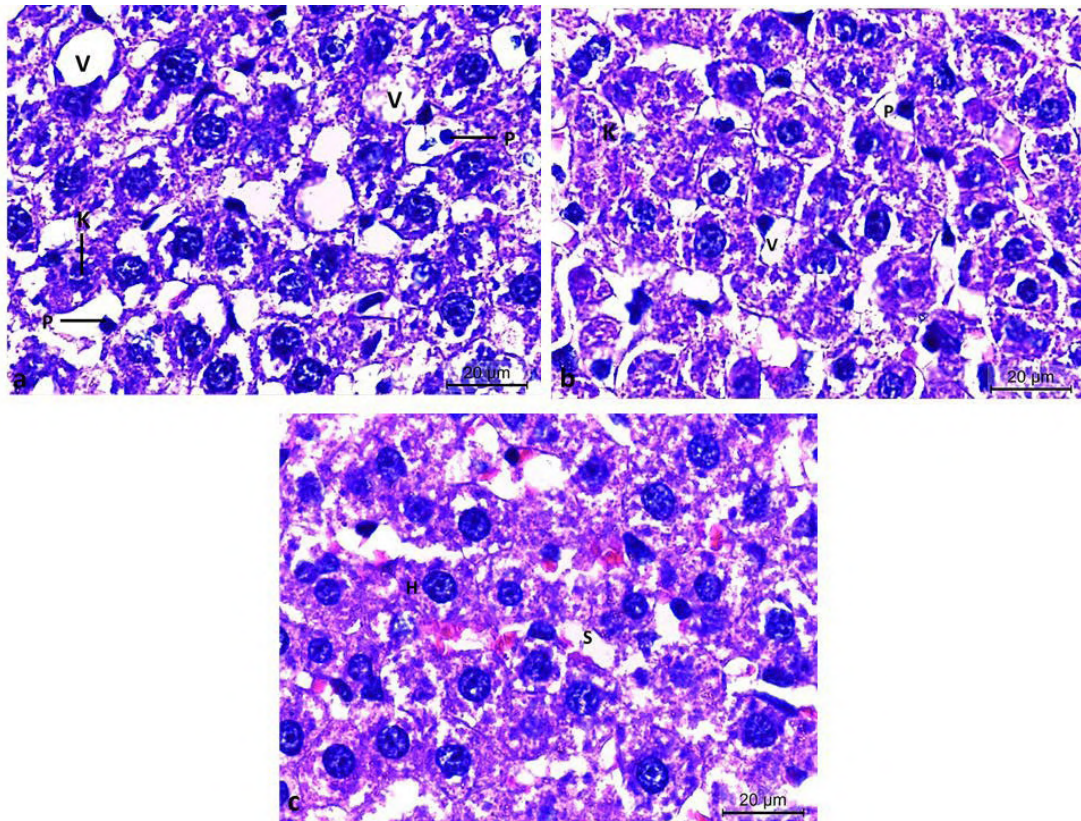


**Fig. 5.-** a and b. Hematoxylin and eosin-stained sections of rat liver in alprazolam-treated group III showing loss of hepatic architecture along with hepatocyte cytoplasmic ballooning and vacuolization (V). Nuclear pyknosis (P) and karyolysis (K) are also featured. c. Hematoxylin and eosin-stained section of rat liver in alprazolam+stem cells-treated group IV showing partial improvement of liver architecture with blood sinusoids (S) intervening between hepatocytes (H). H&E, x1000. Scale bars = 20 μm.

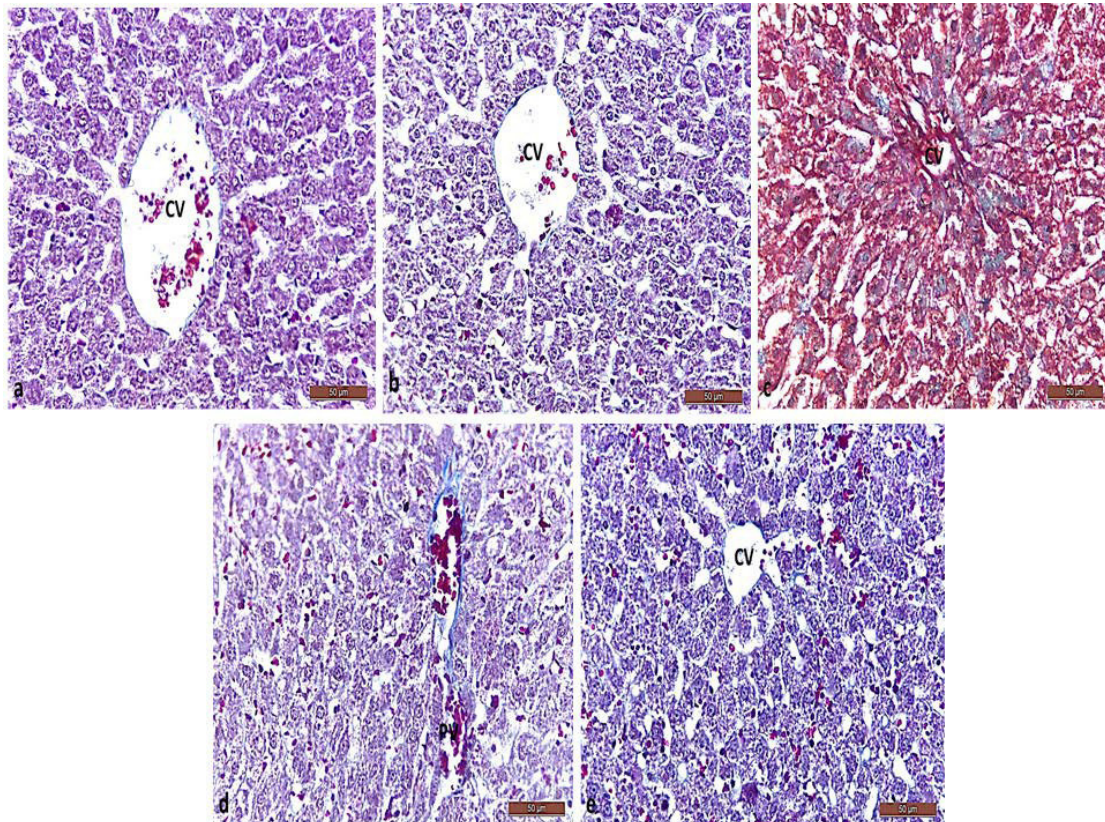


**Fig. 6.-** Masson's trichrome staining for collagen in rat liver sections. a. and b. are normal control and sham control groups I and II. c. and d. Masson's trichrome staining of liver sections in alprazolam-treated group III showing apparent increase in collagen accumulation. Pericentral and periportal fibrosis and deposition of collagen fibers in the hepatic parenchyma are featured. e. Masson's trichrome staining in alprazolam+stem cells-treated group IV showing minimal reaction; central vein (CV), portal vein (PV). Masson's trichrome, x400. Scale bars = 50 μm.

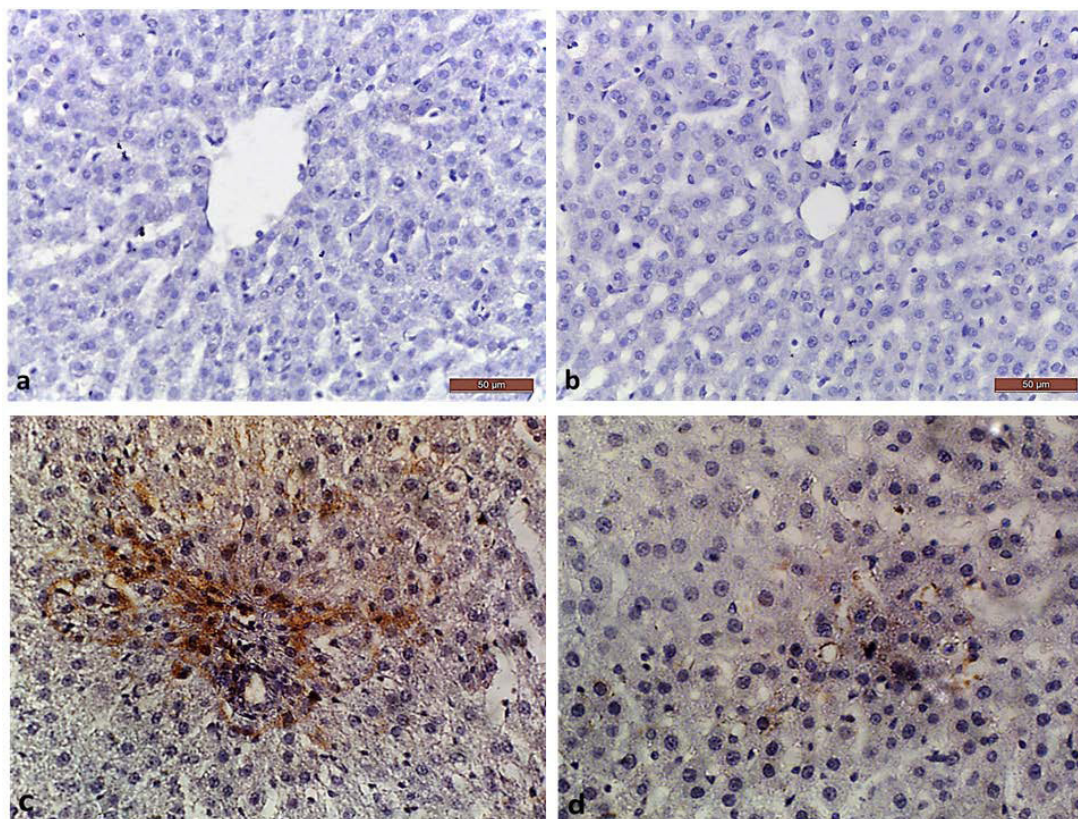


**Fig. 7.-** FGF-2 immunohistochemical analysis of paraffin-embedded rat liver tissue showing negative expression of FGF2 in **a.** control group I and **b.** sham control group II. **c.** FGF-2 immunohistochemical analysis of paraffin-embedded rat liver tissue in alprazolam-treated group III. Marked cytoplasmic localization of FGF2 (score 4) was observed and distributed in large tissue section. **d.** Alprazolam+stem cells-treated rat liver showing mild cytoplasmic localization of FGF2 (score 2). The sections were stained with biotin labelled FGF2 polyclonal antibody (cat no: PMA5-15276), ThermoFisherScientific, USA, followed with DAB staining. Magnification x400. Scale bars = 50 µm.

Very faint alpha-SMA immune-expression was present in control groups I and II (Fig. 8a, b) along the sinusoids. Alpha-SMA immunopositivity markedly increased in alprazolam-treated sections (Fig. 8c, d) as indicated by strong and diffuse brown staining of hepatic parenchyma. A faint expression was seen in alprazolam+stem cells-treated liver sections (Fig. 8e).

### Ultrastructural results

Transmission electron micrographs of liver tissue sections in control and sham control groups I and II showed general architecture of normal hepatocytes. Hepatocytes featured rounded vesicular nuclei, well-formed rough endoplasmic reticulum and mitochondria with few lipid droplets. A regular space of Disse intervened between the hepatocytes and the endothelial cells (Figs. 9 and 10). Hepatic cellular necrosis and vacuolization were seen in alprazolam-treated liver sections. Nuclear chromatinolysis, increased number of lipid droplets and dilatation of space

of the Disse were also seen (Fig. 11). Relative restoration and normalization of hepatocyte architecture were seen in alprazolam+stem cells-treated liver sections (Fig. 12).

### DISCUSSION

In the present study, a non-statistically significant difference in ALT and AST mean serum levels between the control and alprazolam-treated groups was seen. In agreement with the present study, Li et al. (2017) recorded a non-significant difference in alanine aminotransferase and aspartate aminotransferase serum levels between controls and alprazolam groups upon oral alprazolam administration in low, medium and high doses (5, 10 and 20mg/kg/day respectively). In contrast to the present findings, Ibrahim et al., (2017) reported a significant elevation in serum ALT and AST upon oral administration of alprazolam at a dose of 0.3 mg/kg/day. Dutt et al. (2020a) recorded a surge in alanine aminotransferase and aspartate

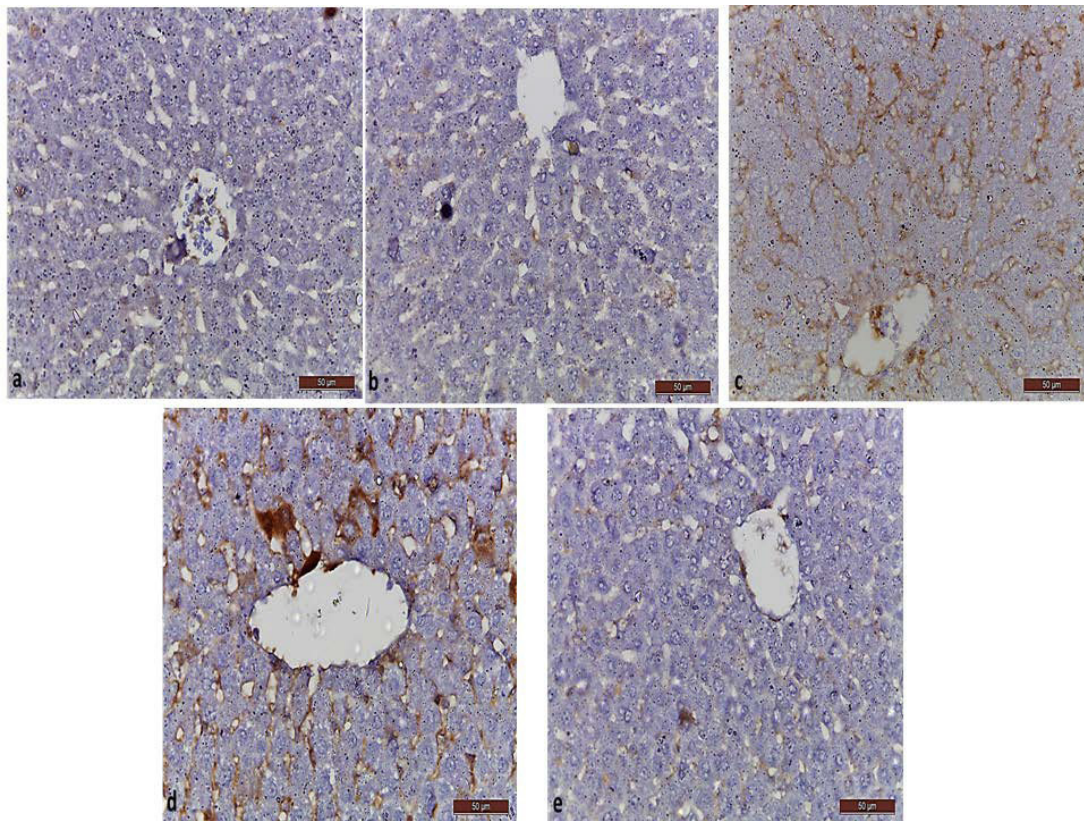


**Fig. 8.-** Immunohistochemical staining of liver sections stained with alpha smooth muscle actin antibody ( $\alpha$ -SMA). **a** and **b** are sections of the control and sham control groups I and II showing negative expression of  $\alpha$ -SMA. **c**, **d**, alprazolam-treated group showing dense brown expression of  $\alpha$ -SMA in between hepatic lobules and into hepatic lobules between hepatocytes (score 4). **e**. Alprazolam+stem cells-treated group showing faint expression of  $\alpha$ -SMA between hepatocytes (score 2). The sections were stained with Mouse Anti-Alpha Smooth Muscle Actin Monoclonal Antibody (Clone 1A4) (CAT#: NAB201062LS), Creative Biolabs, NY, USA. Magnification x400. Scale bars = 50  $\mu$ m.

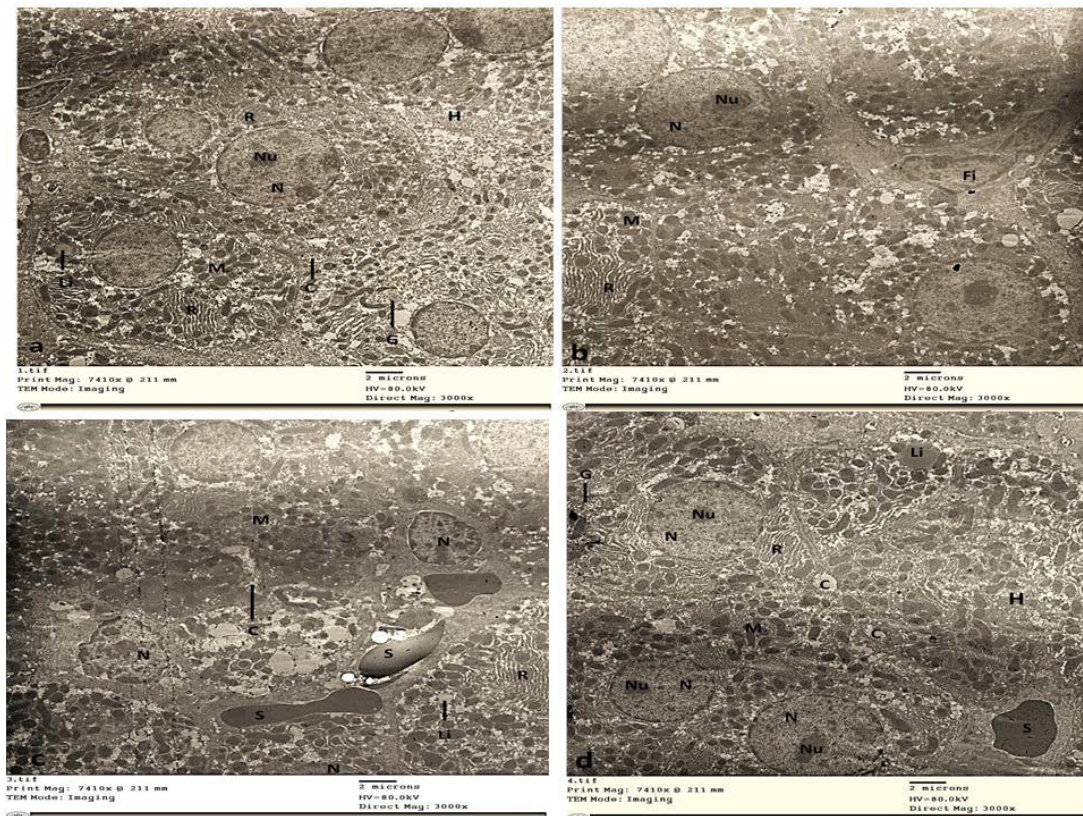


**Fig. 9.-** Transmission electron micrographs of control and sham control rat liver depicting details of hepatocytes (H). Nucleolus (Nu) in hepatocyte nucleus (N); canaliculus (C); rough endoplasmic reticulum (R); glycogen (G); mitochondria (M); lipid droplets (Li.); fibroblast (Fi); blood sinusoid (S) with blood cells in some. Magnification:  $\times 3,000$ . Scale bars = 2  $\mu$ m.

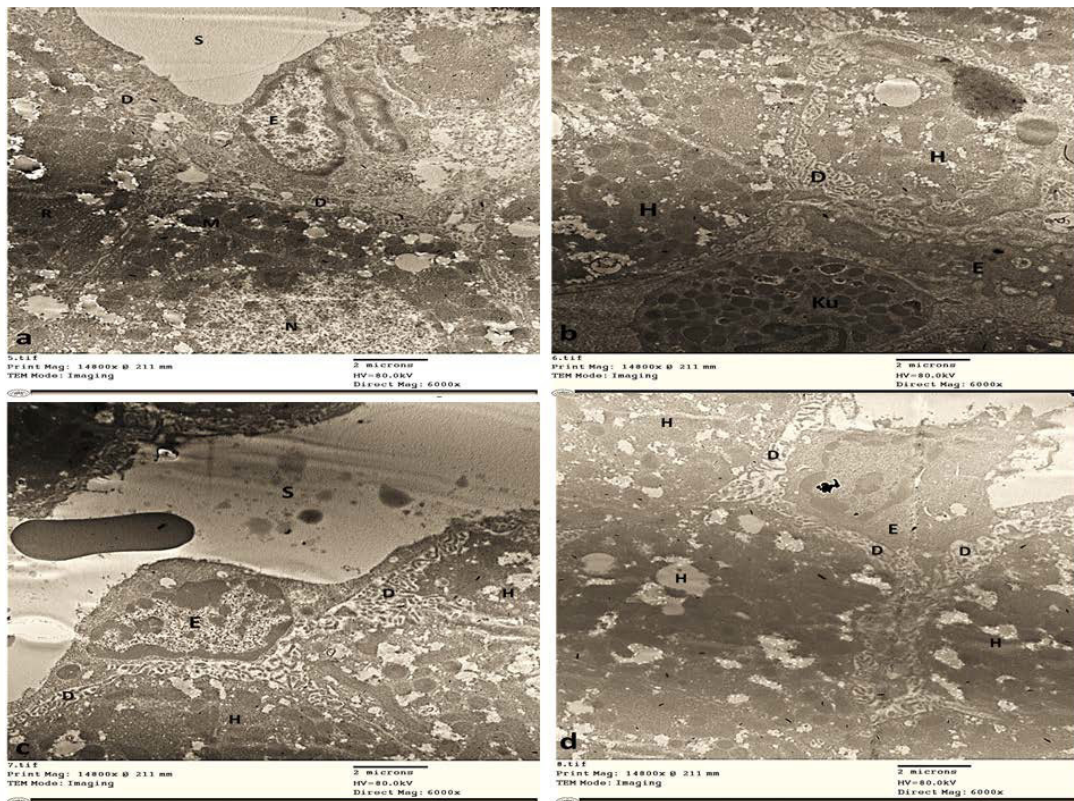


**Fig. 10.-** Transmission electron micrographs of control and sham control rat liver depicting details of hepatocyte (H); hepatocyte nucleus (N); mitochondria (M); blood sinusoid (S) with blood cells in some; endothelial cells (E); space of Disse (D); portion of a Kupffer cell (Ku); Magnification:  $\times 6,000$ . Scale bars =  $2 \mu\text{m}$ .

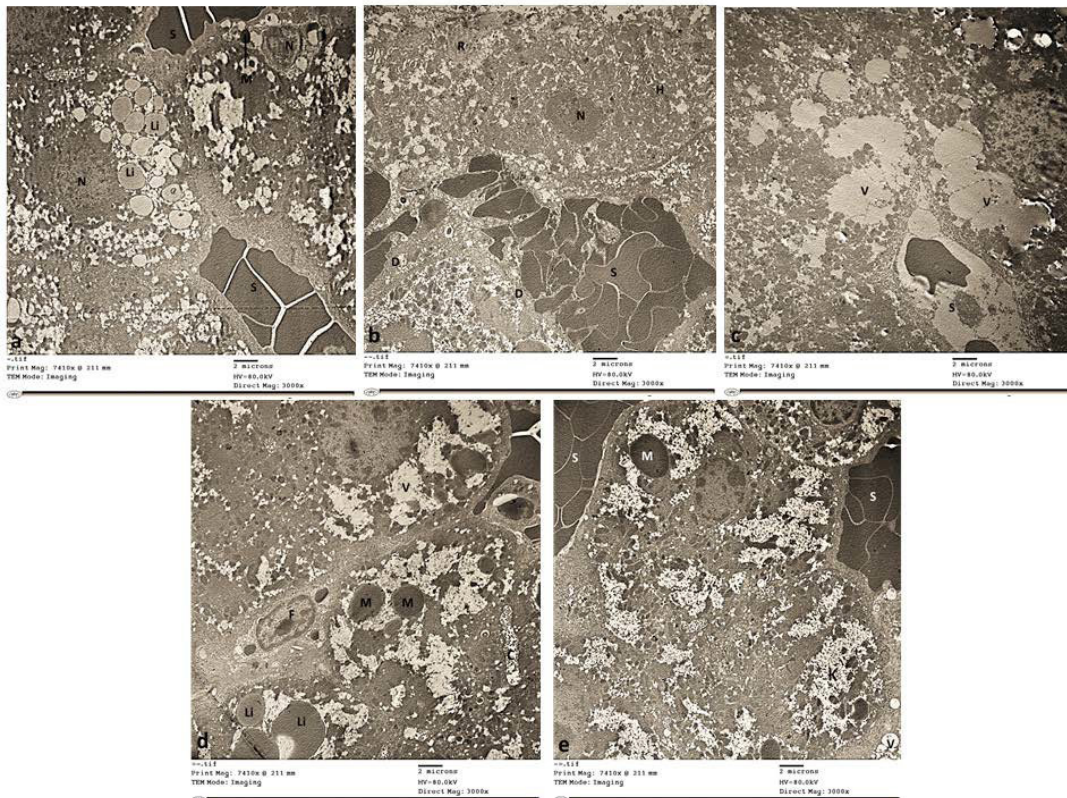


**Fig. 11.-** Electron micrographs of liver tissue obtained from aprazolam-treated rats showing loss of architecture. Hepatocytes are necrotic with large areas of cytoplasmic vacuolization (V) and karyolysis of the nucleus (K). Note the dilated sinusoids (S) filled with red blood corpuscles (RBCs). Necrotic hepatocyte in the centrilobular area with nuclear chromatinolysis (N) and many lipid droplets (Li). Hepatocyte at the periportal region showing fading nuclei with irregular outlines and clumped chromatin (N), swollen mitochondria (M), accumulated lipid droplets (Li), vesiculated rough endoplasmic reticulum (R) and dilated space of Disse (D). Magnification:  $\times 3,000$ . Scale bars =  $2 \mu\text{m}$ .

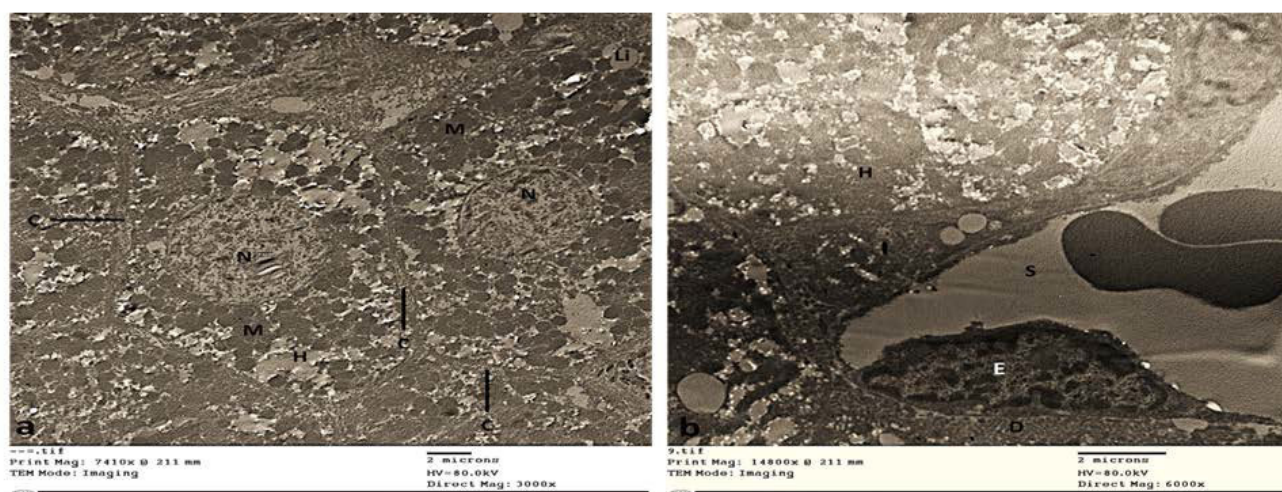


**Fig. 12.-** Transmission electron micrographs of alprazolam+stem cells-treated rat liver depicting normalization of liver architecture with details of hepatocytes (H). Hepatocyte nucleus (N); mitochondria (M) and lipid droplets (Li). Canaliculus (C); blood sinusoid (S) with blood cells in some of them; endothelial cells (E) and space of Disse (D). Magnification:  $\times 3,000$ . Scale bars = 2  $\mu$ m.

aminotransferase serum levels when alprazolam was co-administered with methylphenidate in high doses, whether administered alone or in combination. The authors confirmed that when administered in a low dose, alprazolam caused a non-significant change in the enzyme levels. Dutt et al. (2020b) concluded that the co-administration of alprazolam has augmented the hepato-toxic effects of methylphenidate as proven by the elevated markers for oxidative stress and the reported structural abnormalities in the liver. Dutt et al. (2020a) reported that low, medium and high doses of combined alprazolam and methylphenidate significantly increased lipid peroxidation and decreased SOD levels in liver tissue, whereas in contrast with the current work, the authors stated that individual treatment with alprazolam caused no significant lipid peroxidation except when given in a high dose. According to the authors, the alprazolam-induced reduction in the endogenous SOD levels has augmented the toxic effects of methylphenidate on the liver. The authors suggested that an intercalation of alprazolam with genomic and mitochondrial DNA was a cause for activation of the mechanism involved in cellular death.

In this study, a significant elevation of TNF- $\alpha$  level was seen in the alprazolam-treated group when compared to the control group. In agreement, Dutt et al. (2020b) observed marked increase of neuroinflammation as indicated

by elevated levels of TNF- $\alpha$  following chronic administration of alprazolam when used alone and in combination with methylphenidate to evaluate the extent of damage of both drugs on the brain cortex and hippocampus (Table 2).

Schueller et al. (2018) emphasized the diversified role of miRNAs in maintenance of liver homeostasis, and thus their consequent involvement in acute and chronic liver diseases. The authors reported that knockout of DICER1 in hepatoblast-derived cells leads to a significant downregulation of miRNA-192, among other miRNAs, where development of hepatocytic damage and cellular apoptosis would be seen as a result at 2-4 months of age. MiR-192-5p expression is restricted to hepatocytes. In agreement with the present results, Schueller et al. (2018) revealed a downregulation in intrahepatic expression of miR-192-5p after ischemia and reperfusion (I/R), as well as after CCl<sub>4</sub> induced-liver injury. In contrast, the authors reported an increase in miR-192-5p serum levels after I/R, which was linked with the degree of liver damage and the presence of hepatic cell death. The authors added that downregulation of miR-192-5p had a defensive effect in HepG2 cells after H<sub>2</sub>O<sub>2</sub> treatment, signifying a role of miR-192-5p in preventing liver injury (see Table 2).

Roy et al. (2016) suggested the involvement of miR-192-5p in the control of liver cell death during acute liver injury and considered it to be a potent

marker of hepatic injury. The authors reported a miR-192-5p down regulation in hepatocytes in acute liver injury, with no alteration in its expression among other cell types, indicating a hepatocyte specificity of miR-192-5p regulation during acute liver injury. The authors discussed the role of binding of TNF to its receptor in initiation of signaling cascades which regulate cell cycle or cell death pathways; NF- $\kappa$ B activation being the most prominent pathway. The authors hypothesized that miR-192-5p is regulated by TNF/NF- $\kappa$ B-dependent signaling cascades in hepatocytes and proposed that miR-192-5p is part of a TNF/LPS-dependent signaling pathway that mediates de-repression of anti- apoptotic genes such as Zeb2 defending hepatocytes against cell death in acute liver injury (Table 2).

In accordance with the present results, Andrade et al. (2000) conducted a study that described three patients with benzodiazepines-induced chronic hepatocellular injury, with findings that are indicative of hepatotoxicity of the benzodiazepine, bentazepam. Their findings showed that a benzodiazepine drug can cause chronic hepatitis after oral usage of the drug at a dose of 25 mg twice a day. Percutaneous liver biopsy showed alteration of the hepatic architecture with obvious portal-to-portal fibrosis and transition to cirrhosis as seen with Masson's trichrome staining. Masson's trichrome staining also showed fibrous expansion of portal areas and tracts, fibrous bands surrounding parenchymal regenerative nodes, with bile duct proliferation and inflammatory infiltration, in which mononuclear cells (lymphocytes and plasma cells) dominated. Parenchymal necrosis with acidophilic bodies, regenerative changes, and hepatocytic cholestasis were also noted. The authors hypothesized that bentazepam-related hepatotoxicity has been rarely detected, despite its extensive use, because benzodiazepines are not usually considered as a cause of liver damage. Moreover, chronic hepatitis may be symptomless or its clinical manifestations may be nonspecific, in absence of jaundice. The authors concluded that their findings, together with two previously published case reports, propose that a benzodiazepine can cause chronic hepatitis

and argue in favor of using liver function tests to monitor all patients administered the drug.

**Table 2.** Effect of alprazolam and alprazolam+stem cells on TNF $\alpha$ , SOD and miRNA192 gene expression as compared to the controls.

	Group	Mean $\pm$ SD	Versus	p-value
<b>RQ-TNF-<math>\alpha</math></b>	<b>I</b>	0.89 $\pm$ 0.14	Group II Group III Group IV	1.000 *0.000 *0.001
	<b>II</b>	1.13 $\pm$ 0.32	Group I Group III Group IV	1.000 *0.000 *0.001
	<b>III</b>	5.12 $\pm$ 0.44	Group I Group II Group IV	*0.000 *0.000 *0.000
	<b>IV</b>	2.86 $\pm$ 0.09	Group I Group II Group III	*0.001 *0.001 *0.000
<b>RQ-SOD</b>	<b>I</b>	0.91 $\pm$ 0.03	Group II Group III Group IV	1.000 *0.000 *0.001
	<b>II</b>	1.10 $\pm$ 0.11	Group I Group III Group IV	1.000 *0.000 *0.001
	<b>III</b>	0.01 $\pm$ 0.79	Group I Group II Group IV	*0.000 *0.000 *0.000
	<b>IV</b>	0.55 $\pm$ 0.83	Group I Group II Group III	*0.001 *0.001 *0.000
<b>RQ-miRNA 192</b>	<b>I</b>	1.06 $\pm$ 0.71	Group II Group III Group IV	1.000 *0.000 *0.001
	<b>II</b>	0.95 $\pm$ 0.17	Group I Group III Group IV	1.000 *0.000 *0.001
	<b>III</b>	0.03 $\pm$ 0.87	Group I Group II Group IV	*0.000 *0.000 *0.000
	<b>IV</b>	0.44 $\pm$ 0.62	Group I Group II Group III	*0.001 *0.001 *0.000

\*p value  $\leq$  0.05 was deemed statistically significant; RQ=Reverse Transcription Quantitation; SD=standard deviation.

In the present study, homing of MSCs in liver hepatocytes was verified through the detection of MSCs labeled with PKH26 by fluorescence microscopy. In line with the present study, El Asmar et al. (2011) reported that the generation of

parenchymal damage is a requirement for effective homing and repopulation of stem cells. The authors mentioned that although molecular mechanisms for stem cells mobilization and homing in the injured liver were poorly understood, possible pathways have been proposed including; Stromal Cell-Derived Factor-1 (SDF-1)/CXCR4 axis, the proteolytic enzymes matrix metalloproteinases (MMPs), the hepatocyte growth factor (HGF) and the stem cell factor (SCF) where the Chemokine Stromal Cell-Derived Factor-1 (SDF-1) is considered to be a commanding chemo-attractant of hepatic stem cells' homing, migration, proliferation, differentiation and survival. Aliotta et al. (2007) also discussed the mechanisms involved in bone marrow-derived cells (BMDCs) trans-differentiation triggered by tissue injury. Chemokines produced by tissue injury attract BMDCs, producing microvesicles which are then taken up by BMDCs altering the cell phenotype to mimic resident cells.

Ishikawa et al. (2006) stated that growth factors affect cell proliferation and differentiation and allegedly contribute in repair processes of various organs. The authors reported that transplanted GFP-positive bone marrow cells (BMCs) differentiate into hepatocytes via hepatoblast intermediates. The authors also reported that FGF2 assists the differentiation of transplanted BMCs into albumin-producing hepatocytes via Liv2-positive hepatoblast intermediates through the activation of TNF- $\alpha$  signaling. The authors found that co-administration of FGF2 and bone marrow transplantation (BMT) improves liver function and prognosis of mice with liver injury. Padrisa-Altés et al. (2015) used siRNA delivered via nanoparticles and liver-specific gene knockout to study Fgfr role in liver regeneration. The authors reported that normally Fgf15- Fgfr4-Stat3 signaling pathway is vital for injury-induced expression of the Foxm1 transcription factor and consequent cell cycle progression. The authors observed a failure of liver mass restoration in case of Fgfr4 knockdown in mice, which was compensated for by compensatory hypertrophy of hepatocytes. Knockdown of Fgfr4 in mice lacking Fgfr1 and Fgfr2 in hepatocytes caused liver failure due to severe liver necrosis and a defective

regeneration. The authors recommend activation of Fgfr signaling as a promising approach for the improvement of the liver's regenerative capacity. These results prove that Fgfr signaling in hepatocytes is crucial for liver regeneration and run in agreement with the results of the present study. Kurniawan et al. (2020) reported that FGF2 interacts with FGFR1 which is highly overexpressed in human liver myofibroblasts. The authors suggested different FGF2-regulated signaling pathways including Janus kinase (JAK), signal transducer and activator of transcription (STAT), extracellular signal regulated kinase (ERK), mitogen-activated protein kinase (MAPK), c-jun N-terminal kinase (JNK) and serine/threonine kinase AKT (also known as protein kinase B, PKB) pathways. The authors added that selective inhibitor of phosphatidylinositol 3-kinase (PI3K) and mitogen-activated protein kinase (MAPKK or MEK) eliminate the protective effects of FGF2, proposing involvement of PI3K/AKT and MEK/ERK signaling pathways in FGF2-mediated effects.

In the present work, alpha-SMA immunopositivity was markedly increased in alprazolam-treated group III. Caprino et al. (2005) mentioned that alpha-SMA expression is a dependable marker of hepatic stellate cells activation, occurring even prior to fibrous tissue formation in chronic hepatitis. The authors confirmed that its expression could be a useful measure for identification of the earliest stages of hepatic fibrosis and monitoring the effectiveness of therapy, whereas later in the disease process, fibrosis deposition would be sustained by other mechanisms. Udomsinprasert et al. (2020) discussed the mechanisms underlying the connection of high expressions of Glypican-3 (GPC-3) and  $\alpha$ -SMA with liver fibrosis. The authors stated that GPC-3 contributes in the regulation of HSCs viability through interacting with hedgehog signaling, which in turn plays a fundamental role in maintaining HSCs viability and activation, which are involved in hepatic fibrogenesis. The authors added that in liver fibrosis, HSCs are activated and transformed into myofibroblasts that secrete several cytokines/growth factors and produce extracellular matrix proteins including  $\alpha$ -SMA. In contrast to the present results, Zhao

et al. (2018) recorded that although present in fibrotic skeletal muscles, the expression of  $\alpha$ -SMA by myofibroblasts is not demonstrable by immunostaining. The authors found that the level of  $\alpha$ -SMA expression by intramuscular fibrogenic cells does not show a positive correlation with the level of collagen gene expression or the severity of skeletal muscle fibrosis in mice with muscular dystrophy. The authors concluded that  $\alpha$ -SMA is not a functional marker of fibrogenic cells in skeletal muscle fibrosis accompanying muscular dystrophy.

The histopathological findings of the present study, associated with alprazolam administration, provided supportive evidence for the biochemical and molecular analyses. The present findings are in line with those of Dutt et al. (2020b), who observed an increase in hepatocyte cellular necrosis and vacuolization in addition to alterations in the morphological arrangement of hepatocytes in liver tissue upon co-administration of alprazolam. Despite reporting liver cell cord disorder and liver cell edema, Li et al. (2017) concluded that alprazolam is not hepatotoxic in terms of pathological findings.

Ishikawa et al. (2006) demonstrated the potentiality of BMCs to differentiate into various cell types, including hepatocytes. The authors reported an elevation of serum albumin level and a reduction in liver fibrosis, following bone marrow transplantation (BMT). According to the authors, the mechanism of BMC plasticity involved cell fusion, nuclear reprogramming or trans-differentiation. In the early stage following BMT, the authors observed that genes known to control morphology, such as homeobox, helix-loop-helix transcription factors, and FGFs were up-regulated. However, in later stages, upregulation involved genes linked with hepatocyte differentiation, such as hepatocyte nuclear factor-4 and glucose-6-phosphatase isomerase. Khalil et al. (2021) conducted a study to assess the therapeutic effect of BM-MSCs in carbon tetrachloride (CCl<sub>4</sub>)-induced liver injury and fibrosis in male rats, relative to standard drugs derived from herbal plants. The authors observed restoration of liver structure and function upon treatment with stem cells in comparison with the standard drugs. BM-MSCs significantly decreased

AST, ALT, TNF- $\alpha$ , and increased SOD levels compared to the positive control and the standard drugs groups, with no significant difference between the BM-MSCs-treated group and the normal group. The authors attributed the decrease in serum level of TNF- $\alpha$  after BM-MSCs treatment to deactivation of macrophages and hepatic stellate cells. Histologically, the authors reported a significant improvement in induced hepatic fibrosis, as scored by the METAVIR scoring system, with restoration of normal liver tissue in the BM-MSCs group. Normal tissue with no collagen proliferation was recorded in the BM-MSCs group, as seen with Masson's trichrome staining. The findings of the present work are in agreement with the above findings. Khalil et al. (2021) stated that BM-MSCs either undergo differentiation in the liver tissue or release cytokines/chemokines, by means of a paracrine mechanism, which help reduce inflammation, fibrosis and oxidative stress. The authors hypothesized that BM-MSCs stimulate hepatic regeneration in liver damage either by generation of de novo hepatocytes by means of trans-differentiation and/or cell fusion, paracrine stimulation of endothelial differentiation and vasculogenesis, antifibrogenic modulation of the stromal micro-environment and secretion of hepatotrophic growth factors. The growth factors enhance cell survival, decrease chronic inflammation and diminish fibrosis by inhibiting extracellular matrix (ECM) production and deposition, stimulating myofibroblasts apoptosis. Xiu et al. (2020) discussed the therapeutic role of BMSCs in the treatment of acute liver injury in down-regulation of serum markers such as AST and ALT and reduction of mortality. The authors confirmed that BMSCs transplantation markedly attenuated liver injury and improved the survival of rats in acute liver injury. The authors also stated that mesenchymal stem cells (MSCs) are regulated by the stromal cell-derived factor-1 (SDF-1)/CXC chemokine receptor-4 (CXCR4) signaling axis, which promotes stem cells migration to the inflammation-associated disease sites consequent to the activation of PI3K/Akt signaling pathway in BMSCs that is downstream of CXCR4.

## CONCLUSION

This study investigated the hepatic injury associated with oral alprazolam administration and the role of BMSCs. The changes in levels of TNF- $\alpha$ , SOD and miRNA192 indicated alprazolam induced-oxidative stress and liver injury, results that were further supported by the immunohistochemical, histological and ultrastructural findings. There were no significant differences for ALT and AST between control and alprazolam groups as regards the biochemical results. The results indicated a reversal in the previously mentioned findings upon administration of BMSCs. In conclusion, studies investigating frequent and prolonged administration of alprazolam are further needed and administration of BMSCs could be recommended as a therapeutic option in conditions involving alprazolam-induced liver injury.

## REFERENCES

- AGGARWAL BB, GUPTA SC, KIM JH (2012) Historical perspectives on tumor necrosis factor and its superfamily: 25 years later, a golden journey. *Blood*, 119(3): 651-665.
- ALIOTTA JM, SANCHEZ-GUIJO FM, DOONER GJ (2007) Alteration of marrow cell gene expression, protein production, and engraftment into lung by lung derived microvesicles: a novel mechanism for phenotype modulation. *Stem Cells*, 25: 2245-2256.
- ANDRADE RJ, LUCENA MI, AGUILAR J, LAZO MD, CAMARGO R, MORENO P, GARCÍA-ESCAÑO MD, MARQUEZ A, ALCÁNTARA R, ALCÁIN G (2000) Chronic liver injury related to use of bentazepam. *Dig Dis Sci*, 45(8): 1400.
- CARPINO G, MORINI S, CORRADINI SG, FRANCHITTO A, MERLI M, SICILIANO M, GENTILI F, MUDA AO, BERLOCO P, ROSSI M, ATTILI AF (2005) Alpha-SMA expression in hepatic stellate cells and quantitative analysis of hepatic fibrosis in cirrhosis and in recurrent chronic hepatitis after liver transplantation. *Digest Liver Dis*, 37(5): 349-356.
- CHATTOPADHYAY A, DARBAR S, SAHA S, KARMAKAR P (2019) Effects of alprazolam administration on the vital organs of adult Wistar albino rats, biochemical and toxicological studies. *Indian J Pharmaceut Educ Res*, 53(1): 127-132.
- DINIS-OLIVEIRA RJ (2017) Metabolic profile of oxazepam and related benzodiazepines: clinical and forensic aspects. *Drug Metab Rev*, 49(4): 451-463.
- DUTT M, DHARAVATH RN, KAUR T, CHOPRA K, SHARMA S (2020a) Differential effects of alprazolam against methylphenidate-induced neurobehavioral alterations. *Physiol Behav*, 222: 112935.
- DUTT M, DHARAVATH RN, KAUR T, KAUR N, CHOPRA K, SHARMA S (2020b) Co-abuse of alprazolam augments the hepato-renal toxic effects of methylphenidate. *Indian J Pharmacol*, 52(3): 216.
- EL ASMAR MF, ATTA HM, MAHFOUZ S, FOUAD HH, ROSHDY NK, RASHED LA, TAHA FM (2011) Efficacy of mesenchymal stem cells in suppression of hepatocarcinogenesis in rats: possible role of Wnt signaling. *J Exp Clin Cancer Res*, 30(1): 1-11.
- ELMESALLAMY GE, ABASS MA, ATTA A, REFAT NA (2011) Differential effects of alprazolam and clonazepam on the immune system and blood vessels of non-stressed and stressed adult male albino rats. *Mansoura J Forensic Med Clin Toxicol*, 19(2): 1-25.
- GOLOVENKO NY, KOVALENKO VN, LARIONOV VB, REDER AS (2020) Dose and time-dependent acute and subchronic oral toxicity study of propoxazepam in mice and rats. *Int J Pharmacol Toxicol*, 8(1): 1.
- HUANG Z, XU Z, WANG H, ZHAO ZQ, RAO Y (2018) Influence of ethanol on the metabolism of alprazolam. *Expert Opinion Drug Metab Toxicol*, 14(6): 551-559.
- IBRAHIM NA, IBRAHIM SS, MANNA FA, ABDEL-WAHAB KG, ALI MA (2017) Selective amelioration of chronic restraint stress effects on IL-6, liver function and erythrocyte indices by alprazolam or the herb valerian extract in rats. *Egypt J Exp Biol (Zool.)*, 13(2): 149-158.
- ISHIKAWA T, TERAJ S, URATA Y, MARUMOTO Y, AOYAMA K, SAKAIDA I, MURATA T, NISHINA H, SHINODA K, UCHIMURA S, HAMAMOTO Y (2006) Fibroblast growth factor 2 facilitates the differentiation of transplanted bone marrow cells into hepatocytes. *Cell Tissue Res*, 323(2): 221-231.
- KHALIL MR, EL-DEMERDASH RS, ELMINSHAWY HH, MEHANNA ET, MESBAH NM, ABO-ELMATTY DM (2021) Therapeutic effect of bone marrow mesenchymal stem cells in a rat model of carbon tetrachloride induced liver fibrosis. *Biomed J*, 44(5): 598-610.
- KOPP JL, GROMPE M, SANDER M (2016) Stem cells versus plasticity in liver and pancreas regeneration. *Nature Cell Biol*, 18(3):238-245.
- KURNIAWAN DW, BOOLJINK R, PATER L, WOLS I, VRYNAS A, STORM G, PRAKASH J, BANSAL R (2020) Fibroblast growth factor 2 conjugated superparamagnetic iron oxide nanoparticles (FGF2-SPIONS) ameliorate hepatic stellate cells activation in vitro and acute liver injury in vivo. *J Control Release*, 328: 640-652.
- LI Y, LIN G, CHEN B, ZHANG J, WANG L, LI Z, CAO Y, WEN C, YANG X, CAO G, WANG X (2017) Effect of alprazolam on rat serum metabolic profiles. *Biomed Chromatogr*, 31(9): e3956.
- LIM JY, LEE JH, YUN DH, LEE YM, KIM DK (2021) Inhibitory effects of nodakenin on inflammation and cell death in lipopolysaccharide-induced liver injury mice. *Phytomedicine*, 81: 153411.
- MAITRA S, SAHA B, SANTRA CR, MUKHERJEE A, GOSWAMI S, CHANDA PK, KARMAKAR P (2007) Alprazolam induced conformational change in hemoglobin. *Int J Biol Macromol*, 41(1): 23-29.
- MÜLLER AM, HUPPERTZ S, HENSCHLER R (2016) Hematopoietic stem cells in regenerative medicine: astray or on the path? *Transfusion Med Hemother*, 43(4): 247-254.
- PADRISSA-ALTÉS S, BACHOFNER M, BOGORAD RL, POHLMEIER L, ROSSOLINI T, BÖHM F, LIEBISCH G, HELLERBRAND C, KOTELIANSKY V, SPEICHER T, WERNER S (2015) Control of hepatocyte proliferation and survival by Fgf receptors is essential for liver regeneration in mice. *Gut*, 64(9):1444-1453.
- PAGET GE, BARNES JM. TOXICITY TESTS. IN: LAURENCE DR, BACHARACH AL (1964) Evaluation of drug activities pharmacometrics. London and New York: Academic Press, pp 134-166.
- ROY S, BENZ F, ALDER J, BANTEL H, JANSSEN J, VUCUR M, GAUTHERON J, SCHNEIDER A, SCHÜLLER F, LOESEN S, LUEDDE M (2016) Down-regulation of miR-192-5p protects from oxidative stress-induced acute liver injury. *Clin Sci*, 130(14): 1197-1207.
- SCHUELLER F, ROY S, VUCUR M, TRAUTWEIN C, LUEDDE T, RODERBURG C (2018) The role of miRNAs in the pathophysiology of liver diseases and toxicity. *Int J Mol Sci*, 19(1): 261.
- SCUTERI A, MONFRINI M (2018) Mesenchymal stem cells as new therapeutic approach for diabetes and pancreatic disorders. *Int J Mol Sci*, 19(9): 2783.
- UDOMSINPRASERT W, ANGKATHUNYAKUL N, KLAIKEAW N, VEJCHAPIPAT P, POOVORAWAN Y, HONSAWEK S (2020) Hepatic glypican-3 and alpha-smooth muscle actin overexpressions reflect severity of liver fibrosis and predict outcome after successful portoenterostomy in biliary atresia. *Surgery*, 167(3): 560-568.
- UEHARA S, UNO Y, NAKANISHI K, ISHII S, INOUE T, SASAKI E, YAMAZAKI H (2017) Marmoset cytochrome P450 3A4 ortholog expressed in liver and small-intestine tissues efficiently metabolizes

midazolam, alprazolam, nifedipine, and testosterone. *Drug Metab Dispos*, 45(5): 457-467.

WANDRER F, LIEBIG S, MARHENKE S, VOGEL A, JOHN K, MANNS MP, TEUFEL A, ITZEL T, LONGERICH T, MAIER O, FISCHER R (2020) TNF-Receptor-1 inhibition reduces liver steatosis, hepatocellular injury and fibrosis in NAFLD mice. *Cell Death Dis*, 11(3): 1-9.

XIU G, LI X, YIN Y, LI J, LI B, CHEN X, LIU P, SUN J, LING B (2020) Sdf-1/cxcr4 augments the therapeutic effect of bone marrow mesenchymal stem cells in the treatment of lipopolysaccharide-induced liver injury by promoting their migration through PI3K/Akt signaling pathway. *Cell Transplant*, 29: 0963689720929992.

ZAREIFOPOULOS N, PANAYIOTAKOPOULOS G (2019) Treatment options for acute agitation in psychiatric patients: Theoretical and empirical evidence. *Cureus*, 11(11): e6152.

ZHAO W, WANG X, SUN KH, ZHOU L (2018)  $\alpha$ -smooth muscle actin is not a marker of fibrogenic cell activity in skeletal muscle fibrosis. *PLoS One*, 13(1): e0191031.